PAPER

Channel dropping via bound states in the continuum in a system of two nonlinear cavities between two linear waveguides

IOP PUBLISHING JOURNAL OF PHYSICS: CONDENSED MATTER
J. Phys.: Condens. Matter **25** (2013) 395304 (9pp) doi:10.1088/0953-8984/25/39/395304

Channel dropping via bound states in the continuum in a system of two nonlinear cavities between two linear waveguides

Evgeny Bulgakov, Konstantin Pichugin and Almas Sadreev

L V Kirensky Institute of Physics, 660036, Krasnoyarsk, Russia

E-mail: almas@tnp.krasn.ru

Received 15 June 2013, in final form 15 August 2013
Published 4 September 2013
Online at stacks.iop.org/JPhysCM/25/395304

Abstract
We show that two nonlinear resonant cavities aligned between two parallel waveguides can support self-induced bound states in the continuum (BSCs). These BSCs are symmetrical relative to an inversion of the waveguides and to inversion of the transport axis. Due to this BSCs can drop an incident wave from one waveguide to another with very high efficiency. We show also that the frequency of the efficient channel dropping can be tuned by injecting power. All these results are in good agreement with numerical solutions of the Maxwell equations in a two-dimensional photonic crystal of GaAs rods holding two parallel waveguides and two defects made of a Kerr medium.

(Some figures may appear in colour only in the online journal)

1. Introduction

In 1929, Von Neumann and Wigner suggested [1] that certain potentials could support spatially localized states within the continuum spectrum, i.e., bound states with energies in the continuum of positive energy states. Their analysis, examined by Stillinger and Herrick [2], for a long time was regarded as a mathematical curiosity because of certain spatially oscillating central symmetric potentials. Later, in 1973 Herrik [4] and Stillinger [3] predicted bound states in the continuum (BSCs) in semiconductor heterostructure superlattices which were observed by Capasso *et al* as a very narrow absorption peak [5]. Examples of BSCs can be more easily found if one goes beyond the one-dimensional Schrödinger equation. In [6] four mechanisms for BSCs were discussed in 2D systems, among which the mechanisms of destructive interference and symmetry were applied and verified in photonics [7–11]. Whatever the mechanism might be, BSCs occur for a special choice of the parameters of the system to give rise to a singular point for transmission [10, 12] which can be interpreted as collapse of the Fano resonance [13]. Nonlinear systems open new page in the BSCs phenomenon. In the framework of a two-level nonlinear Fano–Anderson model it was shown that BSCs might arise in a self-consistent way [14] without the necessity to tune physical parameters as in the linear case. This phenomenon is generic and it was recently applied to photonic crystals with defects made of a Kerr medium [15, 16] and nonlinear crystals [17].

The aim of this paper is to demonstrate that such self-induced BSCs have a practical use providing a channel dropping between two linear waveguides. A number of channel drop devices based on two linear resonant microcavities aligned between two linear waveguides [18–32] have been studied theoretically and experimentally. The cavities, each represented by a single monopole eigen mode, support two resonances of different symmetry. Then a degeneracy of these resonances provides 100% drop efficiency at the resonant frequency [18, 33, 34]. However, the presence of continua of the waveguides lifts this degeneracy. To enforce exact degeneracy of the cavity resonances channel dropping devices (CDDs) involve special designs with inclusions of different materials [19, 25, 30, 35, 36]. Scheuer *et al* [37] proposed an alternative way using two coupled microring resonators with Kerr nonlinearity. The authors presented an all-optical approach for tuning coupled microring resonators with Kerr nonlinearity, using a strong control beam launched into the photonic structure in parallel with the signal beam. In this paper we show that for the case

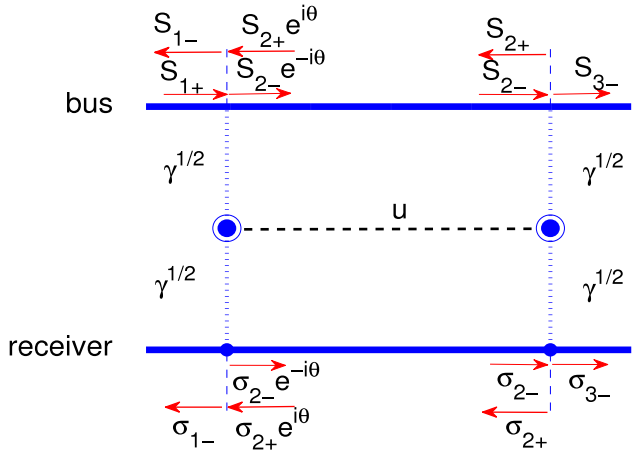

Figure 1. A general four-port system of two coupled identical monopole mode nonlinear cavities between two waveguides. $\gamma^{1/2}$ is the coupling constant between waveguides and cavities coupled via the parameter u.

of two nonlinear cavities the degeneracy of resonant modes is recovered by tuning the light power injected into a bus port to obtain 100% dropping into the receiver port.

2. Basic equations for wave transmission

Let us consider the four-port system shown in figure 1 which consists of two linear waveguides and two nonlinear optical cavities. Following [18] we write the CMT equations with account of the nonlinearity of the two optical cavities,

$$\begin{aligned}[\omega-\omega_0-\lambda I_1+2i\gamma]A_1+[u+2i\gamma e^{i\theta}]A_2 &= i\sqrt{\gamma}S_{1+},\\ [\omega-\omega_0-\lambda I_2+2i\gamma]A_2+[u+2i\gamma e^{i\theta}]A_1 &= i\sqrt{\gamma}S_{1+}e^{i\theta},\end{aligned} \tag{1}$$

where $I_j=|A_j|^2$ are the intensities of the nonlinear cavity oscillations with index $j=1,2$ enumerating the cavities, u is a direct coupling between the cavities and $\omega_0+\lambda I_j$ are the monopole resonant frequencies of the nonlinear cavities. S_{1+} is the amplitude of light injected into the bus waveguide, as shown in figure 1. We complement these equations with equations for the transmission amplitudes,

$$\begin{aligned}S_{3-} &= S_{1+}e^{i\theta}-\sqrt{\gamma}A_1e^{i\theta}-\sqrt{\gamma}A_2\\ S_{1-} &= -\sqrt{\gamma}A_1-\sqrt{\gamma}A_2e^{i\theta}\\ \sigma_{3-} &= -\sqrt{\gamma}A_1e^{i\theta}-\sqrt{\gamma}A_2\\ \sigma_{1-} &= -\sqrt{\gamma}A_1-\sqrt{\gamma}A_2e^{i\theta}.\end{aligned} \tag{2}$$

The CMT equation (1) might be considered as an analogy of the Lippmann–Schwinger equation [35, 15]

$$(\omega-H_{\rm eff})\begin{pmatrix}A_1\\A_2\end{pmatrix}=i\sqrt{\gamma}S_{1+}\begin{pmatrix}1\\e^{i\theta}\end{pmatrix} \tag{3}$$

where

$$H_{\rm eff}=\begin{pmatrix}\omega_0+\lambda I_1-2i\gamma & -u-2i\gamma e^{i\theta}\\ -u-2i\gamma e^{i\theta} & \omega_0+\lambda I_2-2i\gamma\end{pmatrix} \tag{4}$$

is the non-Hermitian effective Hamiltonian. Its complex eigen values for the linear case equal

$$z_{1,2}=\omega_0-2i\gamma\pm(u+2i\gamma e^{i\theta}). \tag{5}$$

The real parts of the eigen values give the resonance positions while the imaginary parts define the resonance widths [40–42]. As was shown in [18], the system operates as a perfect channel drop filter if the resonances are degenerate, $z_1=z_2$, or

$$u=2\gamma\sin\theta,\qquad \cos\theta=0. \tag{6}$$

3. Nonlinear cavities

First, we consider the behavior of the nonlinear CDD in the regime in which a linear CDD would provide a perfect channel dropping, i.e., the parameters satisfy equation (6). Numerically we find two types of solutions. There is the stable solution inherited from the linear case which gives zero reflection, as shown by the dashed line in figure 2(a). The corresponding channel dropping behavior is shown in figures 2(b) and (c). One can see from figure 2(d) that both cavities are excited equally, however with the phase difference $\pi/2$ in full correspondence with [18, 33, 35, 34]. The second type of solution in which the cavities oscillate differently in both the intensities and phases is shown by solid lines in figure 2(d). The existence of at least two types of stable solutions constitutes a difference between the results of [38] where the waveguides are nonlinear and the present system.

In real PhC waveguides the phase $\theta=k(\omega)L$ is very sensitive to the frequency ω, where L is the distance between cavities. Following [15] we approximate the dispersion curve of the PhC waveguide as

$$\theta\approx\pi(\Theta_0+\Theta_1\omega) \tag{7}$$

in the vicinity of resonant frequencies without loss of generality. Again, similarly to the previous dispersionless case there are at least two types of solutions in the vicinity of the phase $\theta=\pi m$ which are drastically different. The first solution which inherits the linear case is shown in figure 3 by dashed lines. However, in some frequency domains a new class of solutions shown in figure 3 by solid lines appears which originates from the bound states in the continuum (BSCs). This class was first demonstrated in a Fabry–Perot interferometer with two nonlinear cavities [15]. In what follows we refer to this class of solutions as the BSC solution for brevity while the solution which inherits the linear case will be defined as the ordinary solution.

In the linear case the BSC introduced first by Von Neumann and Wigner [1] is a localized solution in a specially selected unbounded potential. For a long time the BSC was considered as a mathematical curiosity; however, recently BSCs have been observed in PhC systems [7, 8, 10, 11]. For the description of light with use of the CMT equations, which constitute a version of the Lippmann–Schwinger equation [7, 35], BSCs occur when the matrix of the CMT equation (1) is singular, i.e., $\det[\omega-H_{\rm eff}]=0$ [43]. In what follows we take for simplicity that the

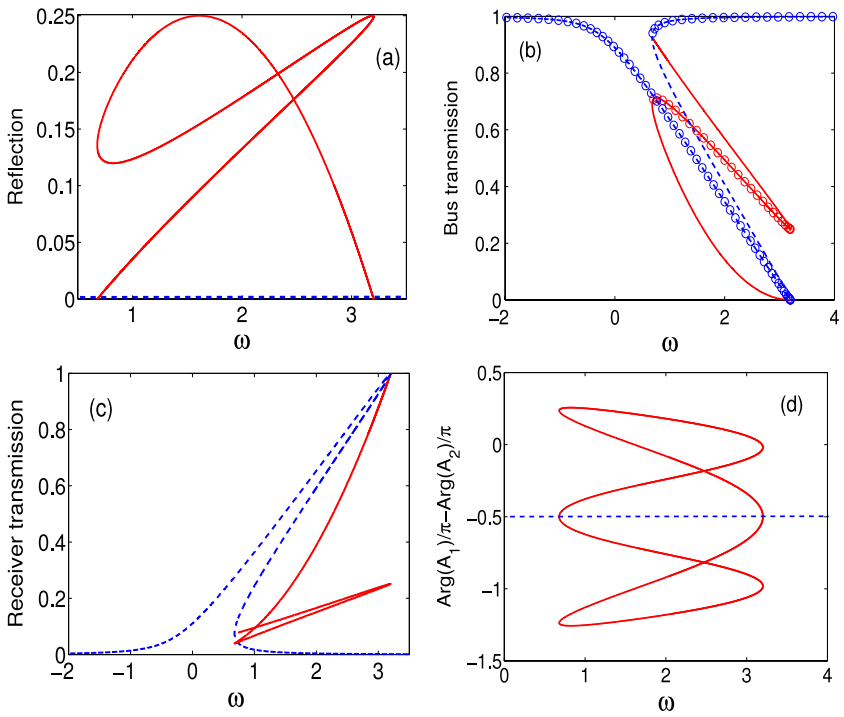

Figure 2. Frequency behavior of (a) the bus reflection, (b) the forward transmission in the bus waveguide, (c) the forward transmission in the receiver waveguide, and (d) the phase difference between the defect amplitudes for the case of non-dispersive waveguides. The model parameters obey the channel drop condition for the linear case (6), $\theta = \pi/2$; the other parameters are $\gamma = 0.0625$, $\lambda = 0.2$, $S_{1+} = 2$, $\omega_0 = 0$, $u = 2\gamma$. Dashed lines mark the solution which reduces to the linear case for $S_{1+} \to 0$. Open circles mark a stability of the solutions.

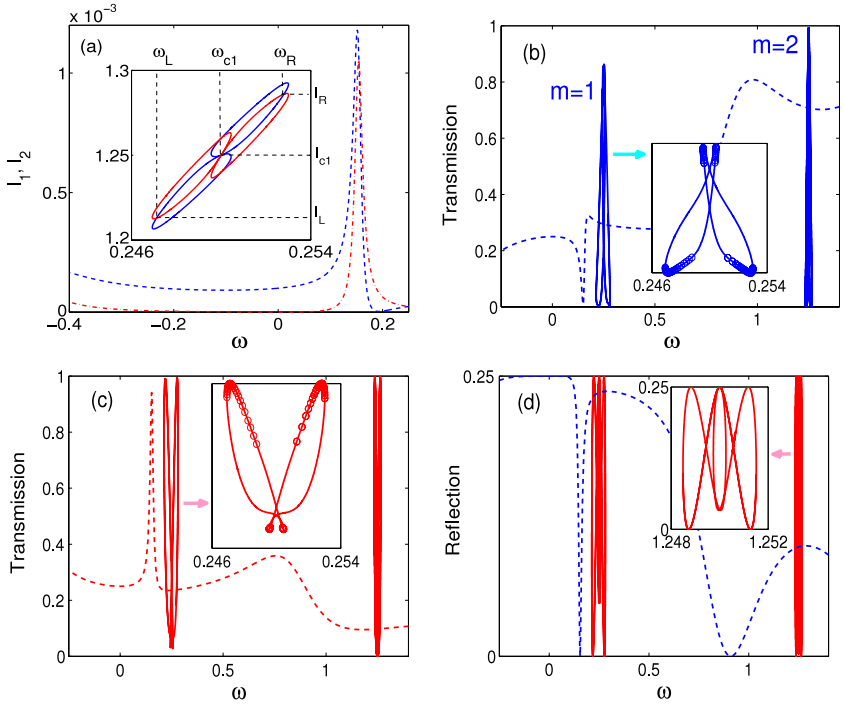

Figure 3. (a) Intensities of mode oscillations at the cavities where the first/second cavity intensity is shown by dashed/dash-dotted lines for the first solution which is inherited from the linear case. The inset shows the second solution where the cavity's intensities are shown by solid lines (red and blue respectively). (b) Transmission to the bus waveguide where the dashed blue line shows a fragment of the bus transmission inherited from the linear case and the solid red line shows the solution related to the BSCs with $m = 1, 2$. (c) The same for the transmission to the receiver waveguide. (d) Bus reflection. The phase difference between cavities follows the rule $\theta = \pi(3/4 + \omega)$. The parameters are chosen as $\lambda = 0.2$, $\gamma = 0.25$, $\omega_0 = 0$, $u = 0$, $S_{1+} = 0.01$.

cavities are far from each other ($u = 0$). Then it is easy to find from equation (1) that BSCs occur for $\omega = \omega_m^{\rm BSC} = \omega_0$ and $\cos\theta = \pm 1$, where $\Theta_0 + \Theta_1\omega_m^{\rm BSC} = m$ and the m are integers. Thus, a BSC arises if the eigen frequency ω_0 is tuned to one of the $\omega_m^{\rm BSC}$ values. Then at $\omega = \omega_m^{\rm BSC}$ one of the resonance widths defined by the imaginary parts of the complex eigen values of the effective Hamiltonian $H_{\rm eff}$ [40] turns to zero. The BSC is the solution of the homogeneous part of the Lippmann–Schwinger equation (1), $(\omega - H_{\rm eff})|{\rm BSC}\rangle = 0$, which equals

$$|{\rm BSC}\rangle = \begin{pmatrix} A_1 \\ A_2 \end{pmatrix} = \begin{pmatrix} 1 \\ -{\rm e}^{{\rm i}\theta_m} \end{pmatrix} \tag{8}$$

where $\theta_m = \pi m$. The BSCs are standing waves between two off-channel defects which become perfect mirrors at the frequencies $\omega = \omega_0$. For these frequencies the total solution of the CMT equation can be present as a superposition [43]

$$|\psi\rangle = \alpha|{\rm BSC}\rangle + \frac{S_{1+}}{4\sqrt{\gamma}}\begin{pmatrix} 1 \\ {\rm e}^{{\rm i}\theta_m} \end{pmatrix}. \tag{9}$$

Here, the first contribution is the localized BSC, and the second term is the particular solution of equation (1) which is the extended state. The second particular contribution gives rise to scattering of the input wave into all four ports of the system while the first particular solution is decoupled from them. Because of this the coefficient of superposition α is arbitrary and can be defined for specific physical processes of excitement of the BSC. Thereby the BSCs are not interesting for the CDD in the linear case [32].

For the nonlinear case there are a few remarkable features which make the BSCs important for channel dropping. The first feature is that a singularity of the CMT matrix, i.e., a BSC, occurs in a self-induced way at the quantized intensities [15]

$$|A_1|^2 = |A_2|^2 = I_m^{\rm BSC} = \frac{\omega_m^{\rm BSC} - \omega_0}{\lambda} \tag{10}$$

and discrete set of frequencies

$$\omega_m^{\rm BSC} = \frac{m - \Theta_0}{\Theta_1} \tag{11}$$

without the need to tune the eigen frequency ω_0. Recently it was established that nonlinearity might give rise to BSCs self-consistently in a generic way [14, 17]. Figure 3 shows the results of numerical solution of the CMT equations (1). The ordinary solution presents usual Bragg type excitement of the cavities and is shown by dashed ($|A_1|^2$) and dash-dotted ($|A_2|^2$) lines. The BSC solution is located around the BSC frequency (11) $\omega_1^{\rm BSC} = 0.25$, $\theta = \pi$ and $I_1^{\rm BSC} = 1.25$, which has the shape of double loops for sufficiently small injecting amplitude S_{1+}. There are similar solutions around other BSC points (11) which are not shown in figure 3(a). Consequent substitution of the solutions into equation (2) gives the frequency behavior of the transmission and reflection shown in figures 3(b)–(d) in which the effects of BSCs with $m = 1$ and 2 are reflected in the form of loops.

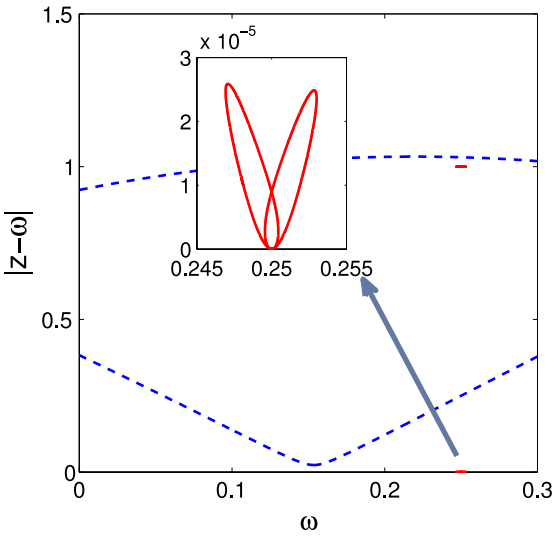

Figure 4. The frequency behavior of the complex eigen values of the effective Hamiltonian (4) for the same parameters as listed in the caption to figure 3. The inset shows a magnification of the frequency behavior $|z - \omega|$ near the BSC point $\omega = 0.25$.

Second, nonlinearity gives rise to an important effect of excitation of a BSC by the propagating wave, i.e., an interaction between the BSC and the propagating wave. This interaction can be expressed by the imaginary parts of the complex eigen values of the effective Hamiltonian $-2{\rm Im}(z)$ which would define the resonance width in the linear case [39, 40]. We have the equality $\det[\omega - H_{\rm eff}] = (z_1(\omega) - \omega)(z_2(\omega) - \omega)$, where $z_{1,2}$ are the complex eigen values of the effective Hamiltonian. The frequency behavior of $|z_{1,2}(\omega) - \omega|$ is presented in figure 4 with substitution of those intensities $I_j = |A_j|^2$, $j = 1, 2$ into equation (4) which correspond to the ordinary solution (dashed lines) and the BSC solution (solid lines) of the CMT equation (1). The latter has the shape of two loops which originate from the BSC frequency $\omega_1^{\rm BSC}$, as the inset to figure 4 shows. For the injected power tending to zero ($S_{1+} \to 0$) the value $|z(\omega) - \omega| = \sqrt{({\rm Re}(z) - \omega)^2 + {\rm Im}(z)^2}$ shrinks to zero for the BSC solution. Therefore, indeed, for the nonlinear case we have $\det[\omega - H_{\rm eff}] = 0$ which defines the BSC. However, as soon as $S_{1+} \neq 0$ the value ${\rm Im}(z)$ differs from zero, i.e., the BSC begins to couple with the continuum of the waveguides in the nonlinear system.

In the vicinity of the BSC frequency $\omega = \omega_1^{\rm BSC}$ we can evaluate the coupling of the BSC with the injected wave. Following [18] we introduce the symmetric and anti-symmetric oscillations $A_{\rm s,a} = \frac{A_1 \pm A_2}{\sqrt{2}}$ and rewrite the CMT equations (1) as follows for $\theta = \pi + \delta$ when δ is small:

$$\begin{aligned} [\omega - \omega_{\rm s} + {\rm i}\Gamma_{\rm s}]A_{\rm s} - \lambda{\rm Re}(A_{\rm s}A_{\rm a}^*)A_{\rm a} &= \sqrt{\Gamma_{\rm s}/2}S_{1+} \\ [\omega - \omega_{\rm a} + {\rm i}\Gamma_{\rm a}]A_{\rm a} - \lambda{\rm Re}(A_{\rm s}A_{\rm a}^*)A_{\rm s} &= {\rm i}\sqrt{\Gamma_{\rm a}/2}S_{1+} \end{aligned} \tag{12}$$

where

$$\begin{aligned} \omega_{\rm s,a} &= \omega_0 \mp 2\gamma\delta + \frac{\lambda}{2}|A_{\rm s}|^2 + \frac{\lambda}{2}|A_{\rm a}|^2, \\ \Gamma_{\rm s} &= \gamma\delta^2, \qquad \Gamma_{\rm a} = 4\gamma. \end{aligned} \tag{13}$$

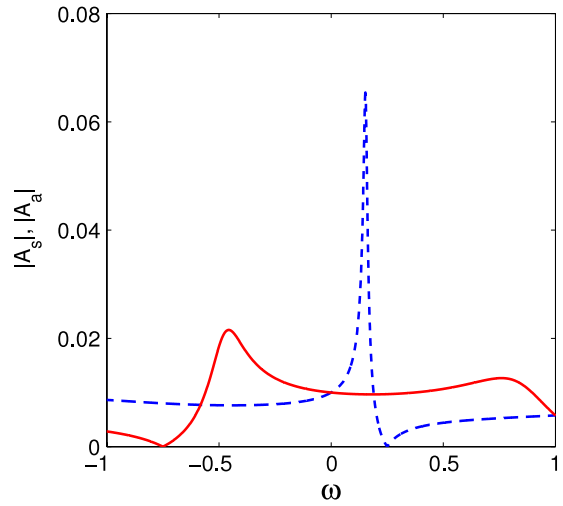

Figure 5. Excitations of symmetric and anti-symmetric modes $A_{s,a} = \frac{A_1 \pm A_2}{\sqrt{2}}$ shown by dash and solid lines respectively. The parameters of the system are the same as in figure 3 $\theta = \pi(3/4 + \omega)$, $\lambda = 0.2$, $\gamma = 0.25$, $u = 0$, $S_{1+} = 0.01$.

For the ordinary solution the symmetric excitation has an extremely small resonance width while the anti-symmetric excitation is rather broad in frequency as figure 5 demonstrates. For the BSC solution we have at the BSC frequency ω_1^{BSC}

$$A_a \approx \frac{S_{1+}}{\sqrt{2\Gamma_a}}, \qquad A_s \approx i\sqrt{\frac{2(\omega_1^{\mathrm{BSC}} - \omega_0)}{\lambda}}. \tag{14}$$

Respectively the solution of equation (12) can be presented as

$$|\psi\rangle = \frac{1}{\sqrt{2}}\left\{A_s\begin{pmatrix}1\\1\end{pmatrix} + A_a\begin{pmatrix}1\\-1\end{pmatrix}\right\}. \tag{15}$$

Comparison of this equation with equation (9) shows that the solution is a superposition of the BSC and an anti-symmetric solution whose amplitude A_a is determined by the injected power as given by equation (14). Therefore the only difference from the linear case is that the amplitude of the BSC A_s is fixed and does not depend on the injected power. From equation (14) one can see also that for the limit to the linear case $\lambda \to 0$ the BSC frequency approaches the frequency ω_0. For the nonlinear case $\lambda \neq 0$ the BSC solution exists in a frequency domain proportional to the injecting amplitude [15]. We can rewrite equation (2) for the receiver transmission amplitude σ_{3-} in terms of the amplitudes $A_{s,a}$ as follows:

$$\sigma_{3-} = \sqrt{\frac{\gamma}{2}}(2A_a + i\delta A_s).$$

Substitution of equation (14) into this equation outlines that the BSC affects the transmission as shown in figures 3(b)–(d). However, what is more important is that this effect plays a key role for channel dropping as we consider next.

Figures 3(b)–(d) show perfect channel dropping not exactly at the BSC frequency ω_1^{BSC} but in a close vicinity of it. Numerics shows that the most effective channel dropping occurs at those frequencies at which the intensities of the mode oscillations coincide, i.e., at the frequency of degeneracy of the nonlinear cavities. For the selected injecting amplitude $S_{1+} = 0.01$ and for the first BSC these frequencies are $\omega_{L,R} = 0.2471, 0.2528$. Let us consider the efficiency of the channel dropping for these frequencies. Substituting the relations for the mode amplitudes $A_j = \sqrt{I_1}\exp(i\phi_j)$ into the CMT equations (1) we obtain $I_1(\omega_0 + \lambda I_1 - \omega_d)^2 = \gamma|S_{1+}|^2$. For small injecting power $|S_{1+}|^2$ we approximate $I_1 \approx I_m^{\mathrm{BSC}}$ where the I_m^{BSC} are given by the quantized set at the BSC points (10) and obtain that $I_m^{\mathrm{BSC}}(\omega_0 + \lambda I_m^{\mathrm{BSC}} - \omega_d)^2 \approx \gamma|S_{1+}|^2$. Then from equation (1) we obtain an equation which relates the phase θ and the phase difference between the mode amplitudes $\phi = \phi_2 - \phi_1$,

$$\exp(-i\phi) = \exp(-i\theta) + \frac{4\gamma\sin\theta}{\omega_d - \omega_0 - \lambda I_1}. \tag{16}$$

The solution is $\phi = \pi - \theta$ where

$$\tan\theta = \frac{\omega_0 + \lambda I_1 - \omega_d}{2\gamma}. \tag{17}$$

As a result, using equations (17) and (2) we obtain finally the forward transmission into the receiver waveguide

$$T_{dw} = \frac{|\sigma_{3-}|^2}{|S_{1+}|^2} \approx \frac{1}{1 + \frac{|S_{1+}|^2}{4\gamma I_m^{\mathrm{BSC}}}}. \tag{18}$$

Respectively, for the transmission into the bus waveguide we obtain from equation (2)

$$T_{\mathrm{up}} = \frac{|S_{3-}|^2}{|S_{1+}|^2} \approx \frac{1}{1 + \frac{4\gamma I_m^{\mathrm{BSC}}}{|S_{1+}|^2}}. \tag{19}$$

These simple formulas show that the efficiency of a CDD based on two nonlinear optical cavities is determined by the ratio $\frac{|S_{1+}|^2}{4\gamma I_m^{\mathrm{BSC}}}$. The larger m is, the larger I_m^{BSC} is, and respectively the efficiency. In particular, for the parameters of the CDD listed in the figure caption we obtain that the efficiency is about 99.8%.

The ordinary solution can also give the efficiency of channel dropping for the eigen frequency of the cavities ω_0 close to the BSC frequency ω_1 for $u = 0$, as shown in figure 3 by dashed lines. However the BSC solution provides more efficiency in the channel dropping than the ordinary solution.

Let us now fix the frequency near the BSC frequency $\omega_1^{\mathrm{BSC}} = 0.25, u = 0$ but vary the injecting amplitude. As seen from figure 6(a) the channel dropping has an efficiency of around 25% for the ordinary solution, which limits to the linear case for $S_{1+} \to 0$. However with growth of the injecting power a narrow peak of extremely high efficiency arises which is the stable BSC solution as shown in figure 6(a). The efficiency falls if the frequency deviates from the BSC point. For large input power the ordinary solution and the BSC solution coalesce to break the CDD regime. These numerical results manifest the most important advantage of nonlinear microcavities, which is the possibility to realize channel dropping by only injecting power without tuning the material

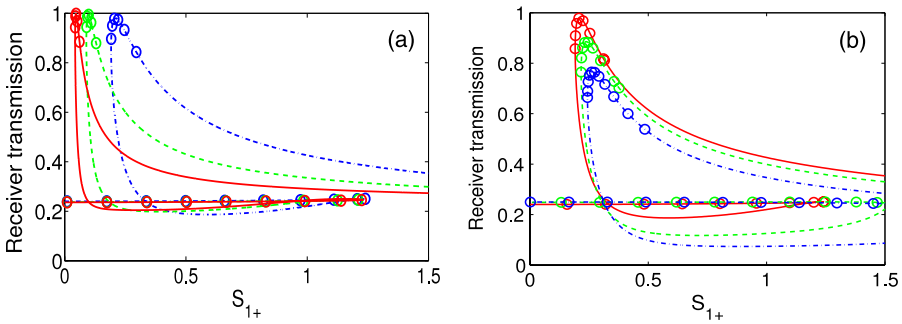

Figure 6. The efficiency of channel dropping as a function of the amplitude of the input light S_{1+} for different values of the frequency $\omega = 0.2625$ (red solid line), $\omega = 0.275$ (green dashed line), and $\omega = 0.3$ (blue dash-dotted line) for zero coupling between the cavities $u = 0$ (a) and for different values of the coupling strength (red solid line), $u = 0.125$ (green dashed line), and $u = 0.25$ (blue dash-dotted line) for fixed frequency $\omega = 0.3$. (b) The other parameters of the system are the following: $\gamma = 0.25$, $\lambda = 0.2$, $\theta(\omega) = \pi(3/4 + \omega)$. Open circles mark the stable domains of the solutions.

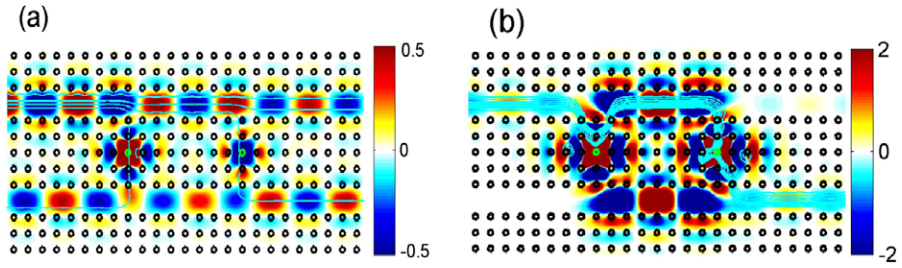

Figure 7. The real part of the scattering wavefunction (electric field) in the PhC, which holds two parallel waveguides and two nonlinear cavities whose monopole eigen frequency $\omega_0 = 0.3447$. The defect nonlinear rods are marked by green open circles. The input power $P_{\text{in}} = 25$ mW$/a$. The light blue lines are optical streamlines which show basic paths for EM power to flow. (a) $\omega = 0.345\,32$ and (b) $\omega = 0.345\,267$. These frequencies are marked in figure 8(a) by a star and a cross, respectively.

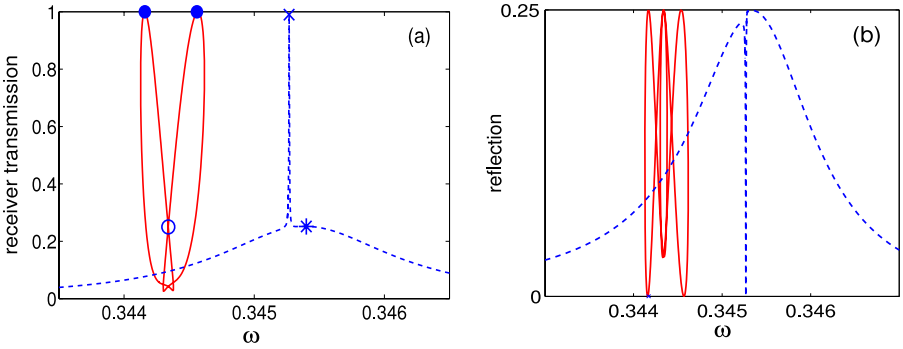

Figure 8. Receiver transmission (a) and reflection (b) as dependent on the frequency of light for $P_{\text{in}} = 25$ mW$/a$ in the PhC configuration shown in figure 7.

parameters of the cavities. The next question is the effect of the coupling strength u on the CDD efficiency. As equation (1) shows, the determinant of the matrix of the CMT equations does not equal zero for $u \neq 0$, i.e., BSCs are excluded. Therefore one can expect that the CDF efficiency falls also with increase of the coupling strength, as figure 6(b) indeed shows. Numerical calculations show that this conclusion does not depend on the choice of frequency.

4. Solutions in photonic crystal with nonlinear defects

Similarly to [7, 16] we consider a square lattice (lattice constant a) of high-index cylindrical dielectric rods with radius $0.18a$ and dielectric constant $\epsilon = 11.56$ (GaAs at the wavelength 1.5 μm) in air. In figure 7 these rods are shown by open bold circles. The background bulk PhC exhibits a TM-polarization (the electric field is parallel to the axis of the cylinder) band gap at $0.302 < \omega < 0.444$ in units of $2\pi c/a$, where c is the speed of light in vacuum [44]. Removing a row of rods creates the single mode PhC waveguide with an effective width of the order of a few a, as shown in figure 7. We evaluated the dispersion of (7) in this specific PhC waveguide as follows:

$$\theta = k(\omega)L \approx \pi[3 + 41.68(\omega - \omega_3^{\text{BSC}})], \qquad (20)$$

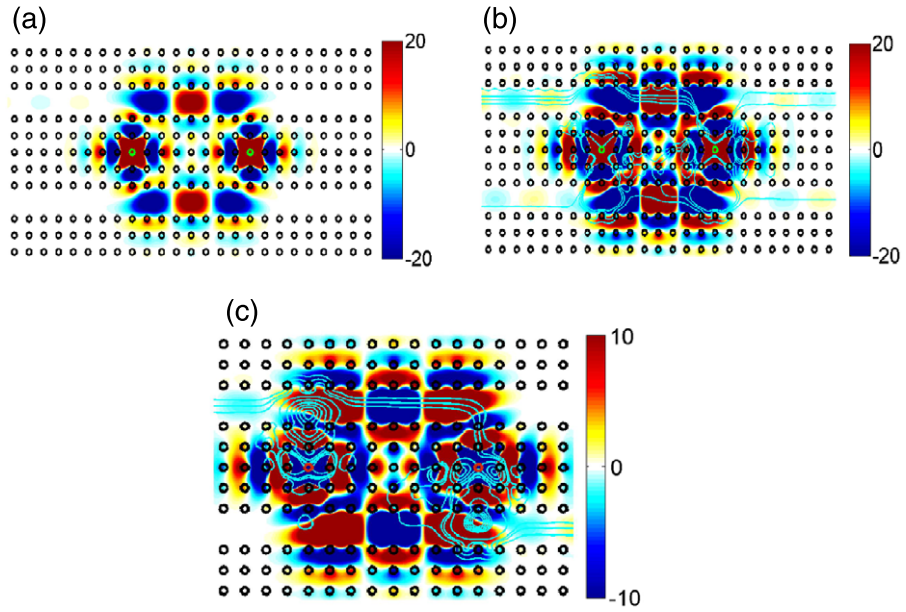

Figure 9. The real parts of the solutions of the Maxwell equations (electric field directed along the rods). (a) The pure BSC at $\omega = \omega_3^{\mathrm{BSC}} = 0.344\,34$ (BSC eigen frequency). (b) The second BSC solution at the BSC frequency marked in figure 8(a) by an open circle. (c) The BSC solution at $\omega = 0.344\,17$ marked in figure 8(b) by closed circles.

$\omega_3^{\mathrm{BSC}} = 0.344\,34$. Localized states are introduced inside the photonic crystal by creating point defects. These point defects can be formed by either changing the radius of a rod compared to the surrounding rods or changing the material of the defect rod. We take the radius of the defect rods to be the same as the other rods but with a linear refractive index $n_0 = \sqrt{3.62}$. Moreover, we consider that the defect rods are made from a Kerr medium with nonlinear refractive index $n_2 = 2 \times 10^{-13}$ cm^2 W^{-1}. Respectively, the nonlinear constant in the CMT equations (1) can be evaluated as follows [16, 45]:

$$\lambda = -\frac{c^2 n_2^2}{a^2} \int_\sigma E_1^2(x, y)\,\mathrm{d}x\,\mathrm{d}y \approx -0.000\,151 \qquad (21)$$

where $E_1(x, y)$ is the monopole eigen mode of the defect cavity, the shape of which could be foreseen for the resonant excitation of the microcavities shown in figure 7(a). σ is the cross-section of the nonlinear defects shown by green open circles in figure 7. We also evaluated other parameters of the PhC system for the eigen frequency $\omega_0 = 0.3447$. The resonant width $\gamma = 0.000\,19$ was obtained directly from the resonant transmission through the PhC waveguide with a side positioned single microcavity calculated by numerical solution of the Maxwell equations for the TM mode propagation. In the linear case in order to satisfy the channel dropping condition (6) it is necessary to tune the dielectric constant of four rods surrounding the defect rods [35], which is a rather delicate procedure. In the case of nonlinear defects, as was shown in section 3, the efficiency can be tuned by the intensity of the injecting light in the region of stability of the BSC solution where $\theta \approx \pi m$.

Here, we show that these results are preserved in 2D PhC too. The method for solving the Maxwell equations is described in the appendix of [45].

The transmission and reflection as dependent on frequency are shown in figure 8. Very similarly to the CMT results we reveal two solutions of the nonlinear Maxwell equations. The ordinary solution shown by dashed lines inherits the linear case and demonstrates forward channel dropping with almost perfect efficiency. However, this occurs in an extremely narrow frequency domain which makes the solution difficult for potential applications. In figure 7 we present the ordinary solution of the nonlinear Maxwell equations in the form of the real part of the electric field for TM polarization for two frequencies. Details of the calculation of the scattering wavefunction are given in the appendix of [45]. At the first frequency $\omega \approx 0.345\,32$, which is marked by a star in figure 8(a), the bus and receiver transmission and reflection approximately equal 0.25. Respectively, figure 7(a) shows that this occurs because of weak excitation of the anti-symmetric cavity's mode. This observation agrees with the CMT consideration presented in figure 5(b) by the solid line. Figure 7(b) demonstrates that resonant excitation of the symmetric cavity's mode gives rise to perfect channel dropping. The streamlines [46] in figure 7(b) clearly demonstrate this result.

In figure 9 we present three patterns for the BSC solution of the nonlinear Maxwell equations. The first pattern shows the self-induced pure BSC which takes place when there is no light injected into the system and $\omega = \omega_3^{\mathrm{BSC}} = 0.344\,34$. This frequency is marked by an open circle in figure 8(a). Differently from the linear case the BSC has a definite discrete intensity with correspondence to equation (10). Because of the small nonlinearity constant (21) one can see that the amplitude of the BSC is rather high compared to the injecting amplitude. Moreover, the pure BSC is a symmetric state which is fully decoupled from the four continua of the four ports of the system.

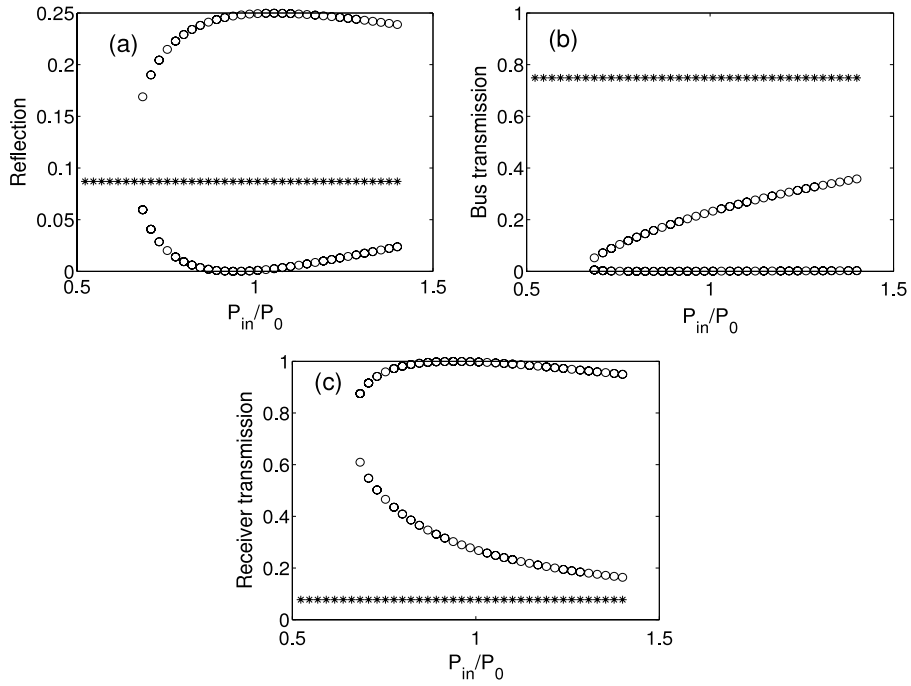

Figure 10. Reflection and transmission versus input power P_{in} normalized by the power $P_0 = 25$ mW$/a$ for $\omega = 0.344\,164$ in the 2D PhC CDD structure shown in the figure. Open circles mark the BSC solution while stars mark the ordinary solution.

Figure 9(b) demonstrates the transport solution at the same BSC frequency. In full accordance with equation (15) we see that the BSC dominates in the transmission because of its large intensity. Nevertheless there is a contribution of the anti-symmetric mode A_{a} to give rise to volatile flows of light between the defects, as seen from figure 9(b). However, the efficiency of channel dropping at this BSC frequency is about 25% only as marked by the open circle in figure 8(a).

The third pattern, figure 9(c), shows the BSC solution at the frequency $\omega = 0.344\,17$ marked by the closed circle in figure 8(a). The coupling of the BSC with the transmitting wave is maximal, as the CMT consideration demonstrates in figure 4. In full agreement with the model CMT consideration we see channel dropping with very high efficiency, as the streamlines demonstrate in figure 9(c). Note that the BSC solution at the second frequency $\omega = 0.344\,54$, also marked by a closed circle in figure 8(a), has no visible difference compared to the pattern in figure 9(c).

There are no other BSCs with the eigen frequencies ω_m^{BSC} because of the finite propagation band of the waveguide for this specified 2D PhC. Finally, we demonstrate that the CDD regime can be achieved by growth of the input power, as demonstrated in figure 10, which was predicted by the CMT consideration (see figure 6). This result presents the important property of the nonlinear cavities as the most promising for CDDs.

5. Summary

In this study we have demonstrated channel dropping between two linear waveguides by use of optical microcavities made from a Kerr medium. The main difference between the mainstream research in this field and the present study is that we exploit the special solution of the nonlinear equations in the form of the bound state in the continuum (BSC). The BSC occurs in the special case when the phase difference between the cavities approaches integers of π. For the considered system the BSC is a standing wave between two off-channel microcavities when the transmission through each defect equals zero (perfect reflection) and the distance between the defects obeys the Fabry–Pérot interferometer quantization condition. For the linear case the BSC occurs in a single point in the space of parameters, and, more importantly, the BSC is not coupled with the injecting light, and thereby cannot be exploited for channel dropping. For the case of nonlinear off-channel microcavities there are a few features which make the BSCs interesting for channel dropping. First of all, the BSCs occur in a self-consistent way [15]. Second, due to the nonlinearity the BSCs couple with the injecting light in the closest vicinity to the BSC frequencies given by equation (11). As a result new sophisticated solutions appear which provide extremely large efficiency of the CDD. The position of perfect channel dropping is governed by the injecting power. More importantly, these solutions are stable.

According to equations (18) and (19) the CDD efficiency in the nonlinear case cannot be 100%, differently from the linear case. However, as figures 6(a) and 10 demonstrate, the efficiency can be extremely high for small injecting power. There is also another feature of the nonlinear case which is the possibility to widen the frequency domain of existence of the BSC solution [15] by the input power. This is important for channel dropping filtering. The third difference between the linear and nonlinear cases is the multiplicity of BSCs that equation (11) shows, and therefore the multiplicity of CDD domains.

The results obtained in the framework of coupled mode theory are in qualitative agreement with direct calculation of the nonlinear Maxwell equations in 2D PhC with two rods made from a Kerr medium between two straightforward waveguides. An extremely high efficiency of channel dropping can be reached. This is a matter of the interplay between the input power, to what extent the frequency of the light is close to the BSC frequency and the coupling constant between the nonlinear optical cavities and the waveguides. Moreover, the mechanism of a CDD based on the nonlinear resonance at the BSC point can be used for all-optical switching of outputs between the bus and the receiver waveguides by applying small pulses to the system.

Acknowledgments

The work is partially supported by RFBR grant 13-02-00497 and Regional RFBR grant 'Sibir' 13-07-98018.

References

[1] Von Neumann J and Wigner E 1929 *Phys. Z.* **30** 465
[2] Stillinger F H and Herrick D R 1975 *Phys. Rev.* A **11** 446
[3] Stillinger F H and Weber T A 1975 *Phys. Rev.* A **10** 1122
[4] Herrik D R 1977 *Physica* B **85** 44
[5] Capasso F, Sirtori C, Faist J, Sivco D L, Chu S-N G and Cho A Y 1992 *Nature* **385** 565
[6] Bulgakov E N and Sadreev A F 2011 *Phys. Rev.* B **83** 235321
[7] Bulgakov E N and Sadreev A F 2008 *Phys. Rev.* B **78** 075105
[8] Marinica D C, Borisov A G and Shabanov S V 2008 *Phys. Rev. Lett.* **100** 183902
[9] Moiseyev N 2009 *Phys. Rev. Lett.* **102** 167404
[10] Lepetit T, Akmansoy E, Ganne J-P and Lourtioz J-M 2010 *Phys. Rev.* B **82** 195307
[11] Plotnik Y, Peleg O, Dreisow F, Heinrich M, Nolte S, Szameit A and Segev M 2011 *Phys. Rev. Lett.* **107** 183901
[12] Sadreev A F, Bulgakov E N and Rotter I 2006 *Phys. Rev.* B **73** 235342
[13] Kim C S, Satanin A M, Joe Y S and Cosby R M 1999 *Phys. Rev.* B **60** 10962
[14] Bulgakov E N and Sadreev A F 2009 *Phys. Rev.* B **80** 115308
[15] Bulgakov E N and Sadreev A F 2010 *Phys. Rev.* B **81** 115128
[16] Bulgakov E N, Pichugin K N and Sadreev A F 2011 *Phys. Rev.* B **83** 045109
Bulgakov E N, Pichugin K N and Sadreev A F 2011 *J. Phys.: Condens. Matter* **23** 065304
[17] Molina M I, Miroshnichenko A E and Kivshar Yu S 2012 *Phys. Rev. Lett.* **108** 070401
[18] Manolatou C, Khan M J, Fan S, Villeneuve P R, Haus H A and Joannopoulos J D 1999 *IEEE J. Quantum Electron.* **35** 1322
[19] Akahane Y, Asano T, Takano H, Song B-S, Takana Y and Noda S 2005 *Opt. Express* **13** 2512
[20] Qiang Z, Zhou W and Soref R A 2007 *Opt. Express* **15** 1823
[21] Song B S, Noda S and Asano T 2003 *Science* **300** 1537
[22] Rokhsari H and Vahala K 2004 *Phys. Rev. Lett.* **92** 253905
[23] Min B K, Kim J E and Park H Y 2004 *Opt. Commun.* **237** 59
[24] Li Z-Y, Sang H-Y, Lin L-L and Ho K-M 2005 *Phys. Rev.* B **72** 035103
[25] Hwang K H and Song G H 2005 *Opt. Express* **13** 1948
[26] Shinya A, Mitsugi S, Kuramochi E and Notomi M 2005 *Opt. Express* **13** 4202
[27] Nawrocka M S, Tao L, Xuang W and Panepucci R R 2006 *Appl. Phys. Lett.* **89** 071110
[28] Xu Q, Sandhu S, Povinelli M L, Shakya J, Fan S and Lipson M 2006 *Phys. Rev. Lett.* **96** 123901
[29] Djavid M, Ghaffari A, Monifi F and Abrishamian M S 2008 *J. Opt. A: Pure Appl. Opt.* **10** 055203
[30] Fasihi K and Mohammadnejad S 2009 *Opt. Express* **17** 8983
[31] Monifi F, Friedlein J, Ozdemir S K and Lan Y 2012 *J. Lightwave Technol.* **30** 3306
[32] Pichugin K N and Sadreev A F 2013 *J. Opt.* **15** 035502
[33] Fan S, Villeneuve P R, Joannopoulos J D and Haus H A 1998 *Opt. Express* **3** 4
[34] Khan M J, Manolatou C, Fan S, Villeneuve P R, Haus H A and Joannopoulos J D 1999 *IEEE J. Quantum Electron.* **35** 1451
[35] Fan S, Villeneuve P R, Joannopoulos J D, Khan M J, Manolatou C and Haus H A 1999 *Phys. Rev.* B **59** 15882
[36] Kim S, Park I, Lim H and Kee C-S 2004 *Opt. Express* **12** 5518
[37] Scheuer J, Sukhorukov A A and Kivshar Yu S 2010 *Opt. Lett.* **35** 3712
[38] Soljačić M, Luo C, Joannopoulos J D and Fan S 2003 *Opt. Lett.* **28** 637
[39] Sokolov V V and Zelevinsky V G 1989 *Nucl. Phys.* A **504** 562
[40] Rotter I 1991 *Rep. Prog. Phys.* **54** 635
[41] Dittes F M 2000 *Phys. Rep.* **339** 215
[42] Savin D V, Sokolov V V and Sommers H-J 2003 *Phys. Rev.* E **67** 026215
[43] Bulgakov E N, Pichugin K N, Sadreev A F and Rotter I 2006 *JETP Lett.* **84** 508
[44] Busch K, Mingaleev S F, Garcia-Martin A, Schillinger M and Hermann D 2003 *J. Phys.: Condens. Matter* **15** R1233
[45] Bulgakov E N and Sadreev A F 2012 *Phys. Rev.* B **86** 075125
[46] Chien C F and Waterhouse R V 1997 *J. Acoust. Soc. Am.* **101** 705